

CrossMark
click for updates

Cite this: DOI: 10.1039/c5ta03214h

Heterojunctions between amorphous and crystalline niobium oxide with enhanced photoactivity for selective aerobic oxidation of benzylamine to imine under visible light†

Yantao Zhang,^{ab} Linjuan Pei,^b Zhanfeng Zheng,^{*b} Yong Yuan,^c Tengfeng Xie,^d Juan Yang,^e Shuai Chen,^b Junwen Wang,^{*a} Eric R. Waclawik^f and Huaiyong Zhu^f

The formation of heterojunctions between two crystals with different band gap structures, acting as a tunnel for the unidirectional transfer of photogenerated charges, is an efficient strategy to enhance the photocatalytic performance of semiconductor photocatalysts. Considering that surface complex photocatalysts also exhibit charge separation and recombination processes, the heterojunctions may also promote the visible-light-response photoactivity of any surface complex catalysts by influencing the transfer of photogenerated electrons. Herein, Nb₂O₅ microfibers, with a high surface area of interfaces between an amorphous phase and a crystalline phase, were designed and synthesised by the calcination of hydrogen-form niobate while controlling the crystallisation. The photoactivity of these microfibres towards selective aerobic oxidation reactions was investigated. As predicted, the Nb₂O₅ microfibres containing heterojunctions exhibited the highest photoactivity. This could be due to the band gap difference between the amorphous phase and the crystalline phase that allows electron transfer unidirectionally, which decreased the recombination rate and improved the efficiency.

Received 5th May 2015
Accepted 20th July 2015

DOI: 10.1039/c5ta03214h

www.rsc.org/MaterialsA

1 Introduction

Imines are important intermediates for the synthesis of fine chemicals and pharmaceuticals.¹ Recently, green processes using light and molecular oxygen to drive the direct oxidation of amines to imines have attracted great attention. Many materials, including metal oxides (*e.g.* TiO₂,^{2,3} Nb₂O₅,^{4,5} BiVO₄⁶, hydrotalcite⁷) and plasmonic metals (*e.g.* Au–Pd⁸ and Ag⁹), have shown high activity and good selectivity for amine to imine conversion. Specifically, the oxidation of amine on Nb₂O₅, a wide band gap semiconductor (~3.2 eV), has shown activity under visible light illumination up to 450 nm which is much narrower than its band gap adsorption at 390 nm.^{4,10–12} It is

reported that the red-shift of the light absorption on Nb₂O₅ is attributed to the formation of a surface complex between the Nb₂O₅ surface and adsorbed amine by forming Nb-amide species.⁴ The surface complex can potentially adsorb light and inject an electron from the N localised on the amide nitrogen into the conduction band of Nb₂O₅ under light illumination using longer wavelengths, which is the so-called ligand-to-metal charge transfer (LMCT) mechanism. Amine itself behaves as a light sensitizer and reactant, and the photocatalyst surface self-regenerates after a reaction cycle. This phenomenon is also observed in TiO₂ (band gap ~3.2 eV) and surface adsorbates that can absorb visible light and initiate reactions.^{13–16} These findings are important because the visible region of the solar spectrum is more abundant than the UV region, which account for 43% and 4% of the solar energy incident on the surface of the earth.¹⁷ In general, shifting the light absorption of wide band gap semiconductors (*e.g.* TiO₂) to the visible range is difficult. Often, lattice doping with metal and non-metal elements is applied for this purpose; however, the loss of the dopant element during recycling is a big concern.^{18–20} Herein, the formation of a surface complex may provide an option to achieve high photoactivity in the visible light range.

In a semiconductor photocatalytic system, the phase junction between two semiconductors acts as an efficient electron and hole separator. It hinders the recombination process and improves the photoactivity.^{21–27} The effect of a surface complex

^aCollege of Chemistry and Chemical Engineering, Taiyuan University of Technology, Taiyuan 030024, China. E-mail: wangjunwen@tyut.edu.cn

^bState Key Laboratory of Coal Conversion, Institute of Coal Chemistry, Chinese Academy of Sciences, Taiyuan 030001, China. E-mail: zfzheng@sxicc.ac.cn

^cXi'an Thermal Power Research Institute Co. Ltd, Xi'an 710032, China

^dCollege of Chemistry, Jilin University, Changchun 130012, China

^eDepartment of Physics and Chemistry, Henan Polytechnic University, Jiaozuo 454003, China

^fSchool of Chemistry, Physics and Mechanical Engineering Queensland University of Technology, Brisbane, QLD 4000, Australia

† Electronic supplementary information (ESI) available: Output spectrum of LED light, normalised photocatalytic activity using the same surface area. See DOI: 10.1039/c5ta03214h

in conjunction with the heterojunction may yield a photocatalyst with high activity by suppressing recombination on the catalyst surface. To form a heterojunction, there needs to be a band gap match between the two phases. In a previous report, we prepared niobate fibres by a hydrothermal method and found that the cations in the structure are exchangeable with other cations.²⁸ Therefore, exchange with H⁺ cations and deliberate control of the calcination temperature can release water from the structure and develop a route to prepare Nb₂O₅ with phase junction structures and thus tune the photocatalytic activity. This procedure is comparable to the phase transformation that occurs during calcination of protonated titanate.²⁴

In the present study, in order to study the structural influence on the photoactivity, niobium oxide (Nb₂O₅) microfibrils were prepared by the calcination of hydrogen-form niobate (H-niobate) at temperatures ranging from 400 to 600 °C to serve as photocatalysts for the selective oxidation of benzylamine to the corresponding imine. It was found that the sample obtained after being calcined at 500 °C generates a mixed phase of amorphous and crystalline Nb₂O₅. This form of Nb₂O₅ microfibrils exhibited much higher activity than the pure amorphous phase and crystalline phase and all demonstrated high selectivity to imine.

2 Experimental

2.1 Catalyst preparation

All chemicals were from Sinopharm Chemical Reagent Co. Ltd unless otherwise stated. Hydrogen-form niobate (H-niobate) microfibrils were prepared by an alkaline hydrothermal treatment of Nb₂O₅ powders and a subsequent ion exchange process. In a typical synthesis, 1.0 g of Nb₂O₅ (AR, Aladdin) was dispersed in a 60 mL aqueous solution of 10 M NaOH and stirred continuously for 4 h. The obtained mixture was autoclaved at 140 °C for 6 h to yield sodium niobate solids. The white precipitate was recovered by centrifugation and subsequently washed with deionised water to remove adsorbed NaOH (designated as NN). Afterwards, the collected solids were washed with an aqueous solution of 0.1 M HCl to exchange the Na⁺ in the structure with H⁺. This was followed by washing with deionised water again and then solid recovery using centrifugation. The sample was dried in air at 100 °C for 12 h (H-niobate, designated as HN). To prepare niobium oxide microfibrils, H-niobate was calcined at 400, 500, and 600 °C for 3 h (designated as HN-400, HN-500, and HN-600, respectively).

2.2 Characterisation

The transmission electron microscopy (TEM) studies on the samples were carried out on a JEM-2100F microscope operating at 200 kV. The sample powder was dispersed in ethanol by sonication; drops of the suspension were applied onto a copper micro-grid-supported transparent carbon foil and dried in air. The scanning electron microscopy (SEM) images were obtained for the morphology study using a JSM-7001F instrument. X-Ray diffraction (XRD) patterns were recorded on a MiniFlex II

diffractometer with Cu-K α radiation ($\lambda = 1.5418 \text{ \AA}$) and operating in a 2θ range of 10–63° at a scanning rate of 4° min⁻¹. Fourier transform infrared spectroscopy (FTIR) was performed using a Nicolet Magna-IR 550-II spectrometer with KBr pellets. Nitrogen sorption isotherms were measured by a volumetric method on an automatic adsorption instrument (Micromeritics, TriStar II 3020 analyser) at liquid nitrogen temperature (77 K). The specific surface area was calculated by the Brunauer–Emmett–Teller (BET) method from the data in a P/P_0 range between 0.05 and 0.2. To investigate the light absorption and emission behaviour of the samples, the UV-Vis diffuse reflectance (UV-Vis-DR) spectra of the samples were measured on a Shimadzu UV-3600 spectrometer. Thermogravimetric/differential thermal (TG/DTA) analysis was carried out on a Rigaku TG in air with a heating rate of 10 °C min⁻¹. Raman spectra were measured on a Horiba LabRAM HR800 spectrometer equipped with a 514 nm argon laser. The electron spin resonance (ESR) spectra were measured using a JEOL JES-RE2X electron spin resonance spectrometer, conducted at room temperature with the addition of 5,5-dimethyl-1-pyrroline N-oxide (DMPO, BePharm). X-ray photoelectron spectroscopy (XPS) was carried out on a Thermo ESCALAB 250 spectrometer at room temperature by using an Al K α X-ray source ($h\nu = 1486.6 \text{ eV}$). The C 1s peak at 284.6 eV was used as a reference for the calibration of the binding energy scale. Transient photovoltage technique (TPV) characterisation was conducted in air atmosphere and at room temperature on a home-made instrument. The sample was excited with a laser radiation pulse (wavelength of 355 nm and pulse width of 5 ns) from a third-harmonic Nd:YAG laser (Polaris II, New Wave Research, Inc.). The TPV signal was registered by using a 500 MHz digital phosphor oscilloscope (TDS 5054, Tektronix).

2.3 Evaluation of photocatalytic activity

Typically, the photocatalytic selective amine oxidation reactions were carried out at 60 °C in an oxygen atmosphere for 10 h. The reaction system consisted of a catalyst (50 mg) and benzylamine (0.2 mmol) in acetonitrile (5 mL). The incident light source was a 100 W COB white LED. The liquid products were analysed using a Shimadzu 2014C GC with a WondaCap 5 column. The single coloured LEDs (blue and green) were also used as irradiation sources to investigate the influence of light wavelength on the photocatalytic activity (output spectra shown in Fig. S1†).

3 Results and discussion

3.1 Physicochemical properties of Nb₂O₅ microfibrils

The X-ray diffraction (XRD) patterns of the as-obtained sodium niobate (labelled as NN), H-niobate (labelled as HN) and niobium oxide microfibrils (H-niobate calcined between 400 and 600 °C, labelled as HN-400, HN-500, and HN-600) are shown in Fig. 1a. Sodium niobate, a hydrated Na₂Nb₂O₆ phase, can be indexed using a space group $C2/c$ with parameters $a = 1.705 \text{ nm}$, $b = 5.029 \text{ nm}$, $c = 1.654 \text{ nm}$ and $\beta = 113.9^\circ$, which is consistent with the previous report.^{28–31} H-niobate and HN-400 exhibited similar patterns which are obviously in the

amorphous state. This could be due to the disordering of the crystal structure during the proton exchange process. According to the Hard-Soft Acid-Base (HSAB) theory, hard acids bind strongly to hard bases and soft acids bind strongly to soft bases.^{32,33} H^+ and Na^+ cations are both hard acids and bind tightly with H_2O , the hard base, in the interlayer of metal oxides. Hydrated H^+ and Na^+ have radii of 0.28 and 0.358 nm,³⁴ regardless of the fact that H^+ and Na^+ cations have small radii of -0.018 and 0.102 nm.^{35,36} Hydrated H^+ is a smaller cation and thus possesses higher priority in the ion exchange compared to hydrated Na^+ . Meanwhile, hydrated H^+ should have a stronger interaction with the layer compared to hydrated Na^+ due to the small size and may cause the collapse of the layer structure. The periodic crystal structure is destroyed and the amorphous structure of the HN is attained. For HN-500, broad diffraction peaks attributed to the amorphous phase and weak diffraction peaks (001), (100), and (101) attributed to hexagonal phase Nb_2O_5 were observed (matched to PDF Card no. 28-0317). For HN-600, all the characteristic diffraction peaks of hexagonal Nb_2O_5 were well-developed which indicates a better crystallinity. The thermogravimetric/differential thermal analysis (TG/DTA) curves for the H-niobate powders are presented in Fig. 1b. Most of the H_2O evolved from the structure at $T < 350$ °C, which yielded an $\sim 8\%$ mass loss. Only an $\sim 1\%$ mass loss was observed in the range between 350 and 600 °C, which means that a niobium oxide product formed. The only endothermic peak at 540 °C in the DTA curve should be attributed to the phase crystallisation from the amorphous phase to crystalline phase.³⁷ The H-niobate and niobium oxide microfibrils exhibited slightly different UV-Vis absorption, as is shown in the UV-Vis spectra (Fig. 1c). As for a direct band gap semiconductor,

the relationship between the absorption coefficient (α) and the optical band gap energy (E_g) near the band edge follows the formula: $\alpha h\nu = A(h\nu - E_g)^{1/2}$, where $h\nu$ and A are the photon energy and a constant, respectively.^{38,39} The band gap energy of Nb_2O_5 can be obtained by extrapolating the linear part of the plots to the photon energy axis. The calculated band gaps are 3.43, 3.27, 3.14 and 3.07 eV for H-niobate, HN-400, HN-500, and HN-600, respectively. This difference could be due to the quantum size effect.^{40,41} They absorb UV light, reflect visible light and thus exhibit white colour. The Raman spectra of the microfibrils, shown in Fig. 1d, also prove that the microfibrils have a different crystal structure. The spectrum of HN-600 exhibits Raman bands at 692, 314, 230 and 141 cm^{-1} , which is similar to the previous reports.^{28,42} The major band at 692 cm^{-1} is the characteristic band for the structure consisting of NbO_6 octahedra-sharing corners.⁴³ The Raman spectrum of HN-500 is similar to that of HN-600, but with a much weaker intensity due to the different crystallinity. The spectrum of HN-400 exhibited a broad peak at 656 cm^{-1} , which is a big shift of the 692 cm^{-1} band for HN-600. This is indicative of the distorted crystal structure in HN-400.⁴³ Valence band X-ray photoelectron spectroscopy (VB-XPS) is routinely used to measure the valence band edge position of a semiconductor.⁴⁴ From the VB XPS spectra of HN-400 and HN-600 (Fig. 1e), the edges of the maximum energy are the same. The UV-Vis spectra of HN-400 and HN-600 revealed that the band gap difference between them is about 0.2 eV. Therefore, the minimum energy of the conduction band edge of HN-600 should be lower about 0.2 eV than that of HN-400 (Fig. 1f).

The scanning electron microscopy (SEM) images of the samples are shown in Fig. 2. As can be seen, the H-niobate sample exhibits a fibrous morphology with the mean diameter distribution from 0.5 to 2 μm . Upon heating from 400 to 600 °C, the long fibres were slightly broken into shorter fibres. HN-400 is in an amorphous phase and it gradually transformed into a crystalline phase as shown by TEM analysis (Fig. S2†). Interfaces between the crystalline phase and amorphous phase are clearly

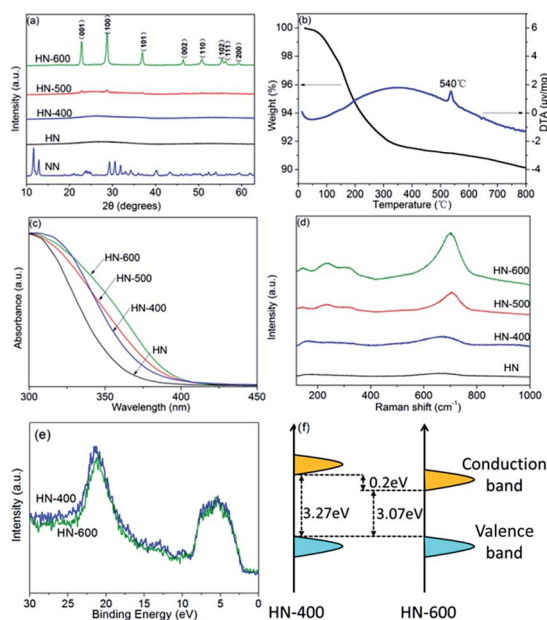


Fig. 1 (a) XRD patterns, (b) TGA-DTA curves, (c) UV-Vis spectra, (d) Raman spectra and (e) valence-band XPS spectra of the microfibrils. (f) Schematic diagram of the DOS of the amorphous and crystalline Nb_2O_5 .

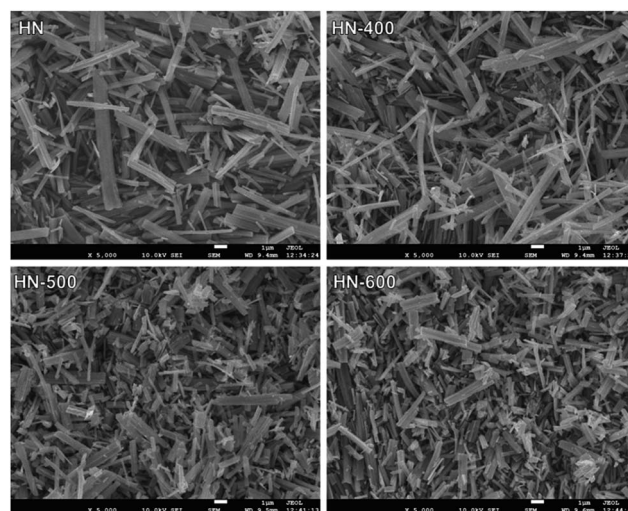


Fig. 2 SEM images of H-niobate and Nb_2O_5 microfibrils. The scale bars are all 1 μm .

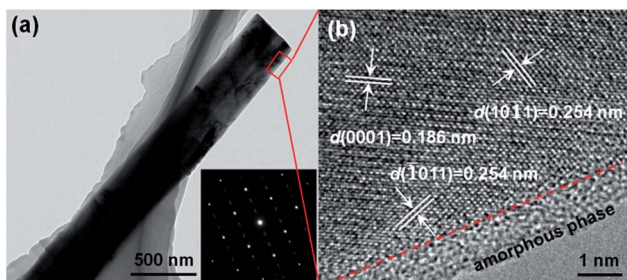


Fig. 3 TEM (a), SAED (inset of a) and HRTEM (b) patterns of a HN-500 microfibre.

seen in HN-500 (Fig. 3). The fringes of (0001), (10 $\bar{1}$ 1) and ($\bar{1}$ 011) planes attributed to hexagonal Nb₂O₅ are indexed to the HRTEM images of HN-500. It is noted that the HN-600 is a single crystal microfibre as shown by TEM observation.

3.2 Photocatalytic performances of Nb₂O₅ microfibres

The photocatalytic performances of H-niobate and niobium oxide microfibres for the selective oxidation of benzylamine are shown in Fig. 4. No conversion was observed in any of the reactions in the absence of light irradiation or O₂, which confirms that the oxidation of benzylamine is a light-driven and dioxygen oxidation reaction. These photocatalysts exhibited very high selectivity (>95%) for the oxidation of benzylamine to the corresponding imine. When the same amounts of catalysts were added, the conversion rate of HN-500 was the highest at 90% (60 °C, 10 h) among the catalysts investigated whose conversion rates were 58% (H-niobate), 80% (HN-400), and 65% (HN-600) and the selectivity was all above 95%. These microfibres had a similar specific surface area at 5.5, 6.7, 5.8, and 5.3 m² g⁻¹ for HN, HN-400, HN-500, and HN-600, respectively. After the specific area of the samples was normalised (using the surface area sample HN-500), HN-500 still exhibited the highest conversion rate at 90%, while HN, HN-40 and HN-600 exhibited a similar rate at 63%, 70%, and 72%, respectively (Fig. S3[†]). The

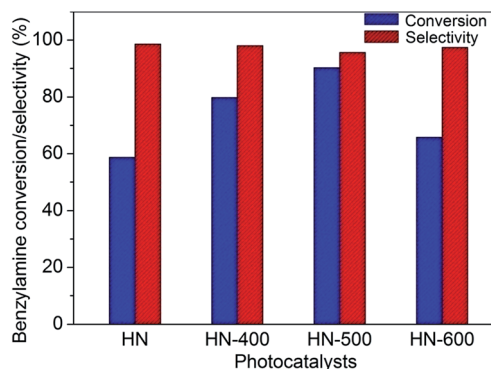


Fig. 4 Performances of H-niobate and Nb₂O₅ microfibers for the selective oxidation of benzylamine under visible light. Reaction conditions: catalyst (50 mg), benzylamine (0.2 mmol), acetonitrile (5 mL), O₂ (1 atm), 60 °C, 10 h, light intensity (0.6 W cm⁻², white LED). No product was observed in the absence of light.

difference between the three catalysts lies in the phase content: HN-400 and HN-600 are in a pure amorphous phase and crystalline Nb₂O₅ phase, respectively, while HN-500 is in a mixed phase with heterojunctions between the two. In the catalytic cycle, an electron is transferred to the conduction band of Nb₂O₅; meanwhile, a hole forms on the surface complex. If the electron is not transferred to an electron acceptor, it recombines with the surface complex to make a null cycle.¹⁴ Therefore, the heterojunction may suppress the hindered recombination process and give a high activity analogous to the recombination process in a semiconductor. It is noted that the recombination process only takes place on the surface, while it happens both in the bulk and on the surface in a semiconductor system.

HN-500 exhibited good recyclability and there is little difference in both relative activity and selectivity after 5 successive cycles (Fig. 5a). The photocatalyst before and after the catalytic reactions was characterised using various techniques including XRD and UV-Vis spectroscopy (Fig. 5b and c). It was found that there is no obvious structure change after the reaction according to the XRD patterns of the sample after 1 cycle, 3 cycles and 5 cycles. After the reaction, the surface of HN-500 was adsorbed with reactants and caused a red-shift in the UV-Vis absorption, and the absorption in the visible range is almost the same for the three reused samples. The vibrations δ_{NH_2} from benzylamine were observed (Fig. S4[†]), and this may indicate that benzylamine is non-dissociatively adsorbed on the oxide surfaces. Niobium oxide does not absorb light of wavelengths larger than 404 nm (the crystalline phase HN-600 has a band gap of 3.07 eV, Fig. 5c). A white-light LED with a wavelength range from 410 nm to 750 nm was used. Therefore, it is reasonable to attribute the activity to the ligand-to-metal charge transfer (LMCT) mechanism. This behaviour has been reported previously by Lang *et al.* who found that anatase TiO₂ could catalyse benzylamine oxidation under visible light illumination.^{2,3} It is believed that the absorbed benzylamine acts as a photosensitiser under visible light illumination, one electron

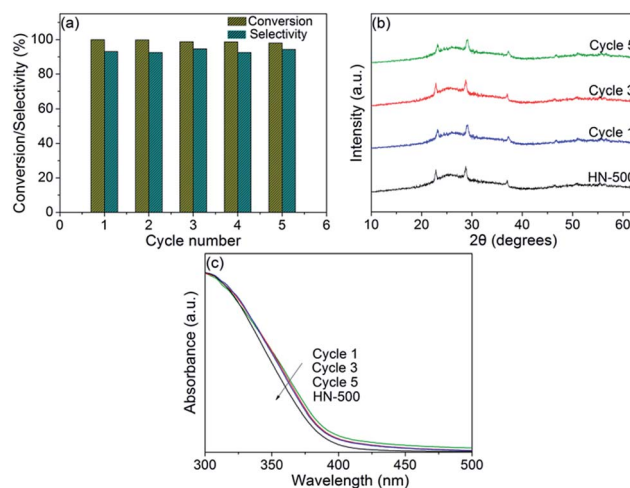


Fig. 5 Recyclability and stability of HN-500 in the benzylamine oxidation reaction. (a) Conversion and selectivity in five successive cycles. (b) XRD patterns and (c) UV-Vis spectra of HN-500 after 1, 3 and 5 reaction cycles. Each cycle was conducted at 80 °C for 8 h.

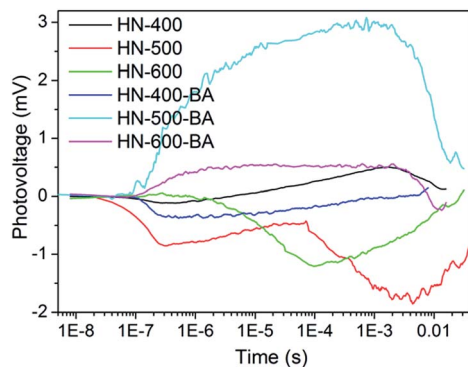


Fig. 6 TPV of HN-400, HN-500 and HN-600 before and after (sample name with suffix "-BA") benzylamine adsorption.

transfers to a single Ti site, and thus the oxidation reaction occurs.

The transient photovoltage (TPV) techniques can provide direct information about the separation and transfer of photo-generated charge carriers in a semiconductor. To understand the transfer properties of the photogenerated electrons, the TPV spectra of the niobium oxide fibers were performed under 355 nm light irradiation and the spectra are shown in Fig. 6. The negative response of photovoltage implies that photogenerated electrons accumulated at the surface and a positive response indicates that photogenerated holes accumulated at the surface.^{45,46} As shown in Fig. 6, the TPV response of HN-400 is negative at the initial period upon light irradiation and it begins to increase and finally a positive TPV response is obtained. This means that photogenerated electrons firstly accumulated at the surface and then photogenerated holes accumulated at the surface. The TPV response of HN-600 is negative, indicating that photogenerated electrons accumulate at the surface of crystalline Nb₂O₅. While for HN-500, the mixed phase sample, a much stronger negative signal was observed compared to the amorphous and crystalline sample (HN-400 and HN-600), which indicates that the heterojunction helps to improve the charge separation.

As for the sample after benzylamine adsorption (sample name with the suffix "-BA"), HN-500-BA, with the heterojunction structure, exhibits a stronger positive response compared to HN-600-BA and HN-400-BA. This means that photogenerated holes accumulated at the surface for the benzylamine adsorbed sample, which is consistent with the LMCT mechanism. The separated electron and hole pair originated from the surface complex is dominant compared to the pair formed due to the Nb₂O₅ bandgap excitation. The TPV response confirms the result that the photogenerated charges have a better separation performance in the sample with the heterojunction structure.

3.3 Photocatalytic mechanism of Nb₂O₅ with heterojunctions

The reaction kinetic data obtained at various temperatures (40, 60 and 80 °C) for the oxidation of benzylamine using HN-500 under visible light irradiation are presented in Fig. 7. It exhibits a typical zero-order kinetic reaction character. The reaction rate

increased gradually when the reaction temperature was increased from 40 to 80 °C. Generally, the recombination rate in a semiconductor photocatalyst increases with temperature, leading to a reduction in the reaction rate.^{47,48} The result observed here further confirms that the complex-route works following a different mechanism. The apparent reaction rate constants (k) of the oxidation of benzylamine on Nb₂O₅ micro-fibres at 40, 60 and 80 °C under visible light irradiation are $3.0 \times 10^{-3} \text{ mol L}^{-1} \text{ s}^{-1}$, $3.9 \times 10^{-3} \text{ mol L}^{-1} \text{ s}^{-1}$ and $5.1 \times 10^{-3} \text{ mol L}^{-1} \text{ s}^{-1}$, calculated from the slope by plotting the curve of conversion vs. the reaction time. Benzylamine was converted to *N*-benzylbenzaldimine with a very high selectivity (>95%) regardless of the reaction temperature. Benzaldehyde was also detected in the product during the reaction which may indicate that benzaldehyde is the intermediate product and converts to imine through a condensation reaction with another benzylamine molecule.³ The estimated apparent activation energy (E_a) for the oxidation of benzylamine using HN-500 is 12.2 kJ mol^{-1} , calculated from the slope of the curve by plotting the reaction rate against $1/T$. It was reported that the apparent activation energy for the selective oxidation of benzylamine to *N*-benzylbenzaldimine on the Au-Pd@ZrO₂ catalyst in the dark and under visible light irradiation was 131.5 and 118.4 kJ mol^{-1} , respectively.⁸ Therefore, the photocatalytic reaction for the oxidation of benzylamine on Nb₂O₅ microfibres has smaller activation energy and can proceed readily. The reaction rate increase with the increasing temperature may indicate that the reaction is a dynamics controlled process, which is due to the increased collision frequency of molecules. In the photocatalytic reports, researchers seldom study the temperature effect.⁴⁹⁻⁵¹ However, both light and heat can speed up the reaction rate and it is important to note that the reaction rate can be greatly improved with a slight increase in the reaction temperature.

The change of either the wavelength or the intensity of the incident light affects the photocatalytic activity of HN-500 (Fig. 8). A higher conversion rate was observed under irradiation of higher intensity. To understand the mechanism, we also studied the dependence of the conversion rate on the irradiation wavelength. Two coloured LED lights [blue (425–510 nm, peaked at 459 nm), green (475–600 nm, peaked at 525 nm), with

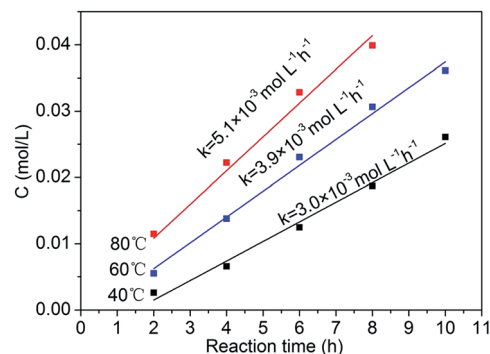


Fig. 7 The reaction profiles in the selective oxidation of benzylamine over HN-500 microfibres at different temperatures (40, 60 and 80 °C).

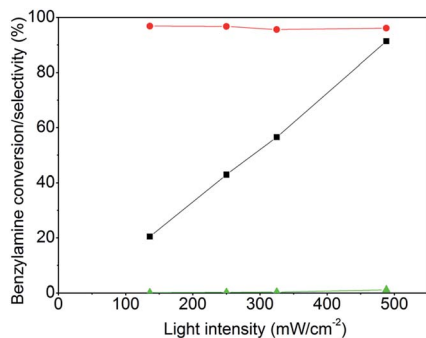


Fig. 8 Light intensity influence of selective oxidation of benzylamine using HN-500 microfibres conducted at 80 °C for 8 h. Conversion of benzylamine (■), selectivity to imine (●) and benzaldehyde (▲).

output spectra shown in Fig. S1†] were used for the wavelength experiments. It was found that HN-500 was active under blue light but did not exhibit any photoactivity under green light. Given that HN-500 has a bandgap of ~ 3.2 eV, the irradiation with wavelength $\lambda > 425$ nm cannot initiate the photocatalytic reaction. Therefore, the catalyst active site under irradiation should be another photocatalytic component – the surface complex. To confirm the radical component formed during reaction, DMPO was introduced into the photocatalytic system and the ESR signal of DMPO-OO(H) was clearly seen (partially decomposed to DMPO-OH, Fig. S5†), which indicates the presence of $\text{O}_2^{\cdot -}$ radicals.⁵²

To understand the substituent influence on the reaction, the catalytic oxidation was conducted on derivative compounds with electron donation groups ($-\text{CH}_3$ and $\text{CH}_3\text{O}-$) and with the electron withdrawing group ($-\text{Cl}$). The results are summarised in Table 1. The substituents on the benzene ring appear to have only a slight influence on the reaction rate and a minor influence on the product selectivity. When a straight chain amine-

Table 1 The influence of substituents on the benzene ring on the reaction rate and selectivity (80 °C, 8 h)^a

Reactant	Product	Conv. (%)	Sel. (%)
		99.98	93.15
		99.61	91.97
		96.12	97.43
		93.59	89.85
	—	quant.	—
		84.26	80.50

^a Conv. = conversion, sel. = selection, quant. = quantitative.

butylamine was used, no imine production was observed in our study. These studies demonstrate that the presence of the benzene ring is important to realise the high conversion during amine oxidation. It is reported that N or C radicals are generated during the reaction process. Therefore, the benzene ring may play an important role in stabilising the adjacent C radical.^{2,5} It is expected that the intermediate product should also be benzaldehyde when an aromatic amine, with more than one C between the benzene ring and the $-\text{NH}_2$ group was used. As expected, when phenethylamine was selected for selective oxidation and the production was found to be 1-phenyl-*N*-(2-phenylethyl)methanimine which is clearly a condensation product of benzaldehyde and phenethylamine.

Based on the above analysis and the previous reports,^{2,3,53,54} we tentatively propose a mechanism for this reaction, as schematically shown in Fig. 9. When the surface complex is irradiated under light, the photogenerated electron injects to the conduction band of Nb_2O_5 , while the hole is left on the surface complex. The hole cannot transfer and the electron can transfer

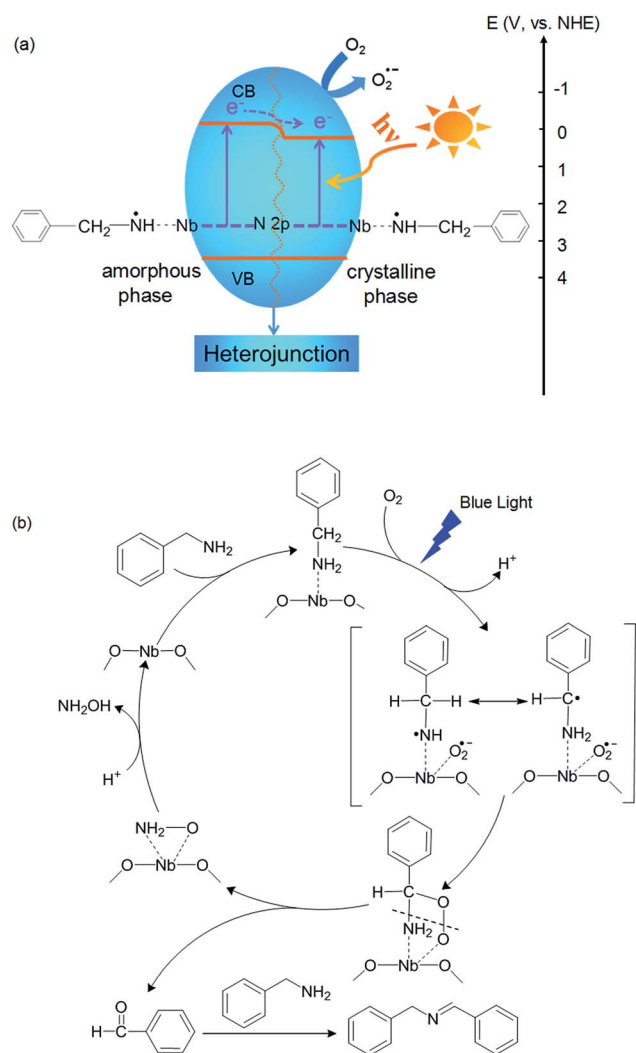


Fig. 9 Schematic illustration of (a) the heterojunction structure and (b) the proposed benzylamine oxidation mechanism of niobium oxide photocatalysts.

between the two phase. Due to the existence of the heterojunction, the net result is that electrons transfer to the crystalline phase with the narrower band gap, which suppresses the recombination process. In a reaction cycle, firstly, the reactant benzylamine is adsorbed on the surface of Nb₂O₅ fibres to form a surface charge transfer complex. Secondly, holes and electrons would be generated on the surface charge transfer complex under light illumination. The photogenerated hole induces H⁺ abstraction from the N of benzylamine and the photogenerated electron transfers to the conduction band of Nb₂O₅, resulting in the activation of molecular O₂ to O₂^{•-}. The nitrogen-centred radical would rearrange *via* intramolecular H-abstraction to form a more stable carbon-centred radical.^{55,56} Thirdly, O₂^{•-} adsorbed on the surface of catalysts forms an intermediate possessing a five-member-ring structure with the carbon radical and Nb⁵⁺ with the termination of the radicals. Fourthly, the cleavage of the C–N bond of benzylamine and the O–O bond of oxygen occurs to form benzaldehyde and a Nb bonded three-member-ring structure. The produced benzaldehyde then further follows a condensation reaction with unreacted benzylamine to yield imine. Finally, the photocatalytic cycle are completed by the regeneration of Nb⁵⁺ sites on the surface of Nb₂O₅ fibres through desorption of the NH₂–OH molecule.

Herein, the Nb₂O₅–amine surface complex structure is significant towards a green synthesis of imine: (1) it can induce a red-shift of the light absorption and improve the light absorption efficiency; (2) it is a self-regeneration process and the active sites can always be “fresh” with the progress of the catalytic reaction; (3) it results in high product selectivity. This process is different from a semiconductor photocatalytic process where the selectivity is very difficult to control due to the high oxidation potential of OH[•] radicals in aqueous photocatalytic systems.^{2,18,57–60}

4 Conclusions

In summary, the amorphous and crystalline phases of Nb₂O₅ microfibres were prepared by the facile calcination of hydrogen niobate at deliberately controlled temperatures ranging from 400 to 600 °C. The Nb₂O₅ microfibres calcined at 500 °C contained heterojunctions between the amorphous phase and the crystallised phase produced during the crystallisation process. It has been found that the surface complexes were formed after amine adsorption on Nb₂O₅, resulting in visible-light photocatalytic activity and enabling direct electron transfer to the conduction band. The catalyst was self-regenerated with the progress of the reaction and exhibited good stability. The heterojunctions effectively improved the photogenerated electron and hole separation efficiency and presented a high conversion rate and product selectivity for the selective oxidation of benzylamine to imine under visible light irradiation.

Acknowledgements

This work was supported by the National Natural Science Foundation of China (No. 51401233), the Advanced Programs of

Department of Human Resources and Social Security of Shanxi Province for Returned Scholars (No. 2013-35), the Shanxi Science and Technology Department (No. 2015081044), and the Hundred Talents Program of the Chinese Academy of Sciences.

Notes and references

- 1 R. A. Sheldon and J. K. Kochi, in *Metal-catalyzed Oxidations of Organic Compounds*, ed. R. A. S. K. Kochi, Academic Press, 1981, pp. 17–32.
- 2 X. Lang, H. Ji, C. Chen, W. Ma and J. Zhao, *Angew. Chem., Int. Ed.*, 2011, **50**, 3934–3937.
- 3 X. Lang, W. Ma, Y. Zhao, C. Chen, H. Ji and J. Zhao, *Chem.–Eur. J.*, 2012, **18**, 2624–2631.
- 4 S. Furukawa, Y. Ohno, T. Shishido, K. Teramura and T. Tanaka, *ACS Catal.*, 2011, **1**, 1150–1153.
- 5 S. Furukawa, Y. Ohno, T. Shishido, K. Teramura and T. Tanaka, *J. Phys. Chem. C*, 2013, **117**, 442–450.
- 6 B. Yuan, R. Chong, B. Zhang, J. Li, Y. Liu and C. Li, *Chem. Commun.*, 2014, **50**, 15593–15596.
- 7 X.-J. Yang, B. Chen, X.-B. Li, L.-Q. Zheng, L.-Z. Wu and C.-H. Tung, *Chem. Commun.*, 2014, **50**, 6664.
- 8 S. Sarina, H. Zhu, E. R. Jaatinen, Q. Xiao, H. Liu, J. Jia, C. Chen and J. Zhao, *J. Am. Chem. Soc.*, 2013, **135**, 5793–5801.
- 9 Z. Zheng, C. Chen, A. Bo, F. S. Zahir, E. R. Waclawik, J. Zhao, D. Yang and H. Zhu, *ChemCatChem*, 2014, **6**, 1210–1214.
- 10 J. He, Y. Hu, Z. Wang, W. Lu, S. Yang, G. Wu, Y. Wang, S. Wang, H. Gu and J. Wang, *J. Mater. Chem. C*, 2014, **2**, 8185–8190.
- 11 Y. Zhao, C. Eley, J. Hu, J. S. Foord, L. Ye, H. He and S. C. Tsang, *Angew. Chem., Int. Ed.*, 2012, **51**, 3846–3849.
- 12 X. Li, N. Kikugawa and J. Ye, *Adv. Mater.*, 2008, **20**, 3816–3819.
- 13 G. Zhang, G. Kim and W. Choi, *Energy Environ. Sci.*, 2014, **7**, 954.
- 14 S. Kim and W. Choi, *J. Phys. Chem. B*, 2005, **109**, 5143–5149.
- 15 S. Higashimoto, N. Kitao, N. Yoshida, T. Sakura, M. Azuma, H. Ohue and Y. Sakata, *J. Catal.*, 2009, **266**, 279–285.
- 16 R. Li, H. Kobayashi, J. Guo and J. Fan, *J. Phys. Chem. C*, 2011, **115**, 23408–23416.
- 17 Z. Zou, J. Ye, K. Sayama and H. Arakawa, *Nature*, 2001, **414**, 625–627.
- 18 A. L. Linsebigler, G. Lu and J. T. Yates, *Chem. Rev.*, 1995, **95**, 735–758.
- 19 R. Asahi, T. Morikawa, T. Ohwaki, K. Aoki and Y. Taga, *Science*, 2001, **293**, 269–271.
- 20 M. Anpo and P. V. Kamat, *Environmentally Benign Photocatalysts: Applications of Titanium Oxide-based Materials*, Springer, London, 2010.
- 21 D. C. Hurum, A. G. Agrios, K. A. Gray, T. Rajh and M. C. Thurnauer, *J. Phys. Chem. B*, 2003, **107**, 4545–4549.
- 22 D. Yang, H. Liu, Z. Zheng, Y. Yuan, J. Zhao, E. R. Waclawik, X. Ke and H. Zhu, *J. Am. Chem. Soc.*, 2009, **131**, 17885–17893.
- 23 J. Zhang, Q. Xu, Z. Feng, M. Li and C. Li, *Angew. Chem., Int. Ed.*, 2008, **47**, 1766–1769.

- 24 Z. Zheng, H. Liu, J. Ye, J. Zhao, E. R. Waclawik and H. Zhu, *J. Mol. Catal. A: Chem.*, 2010, **316**, 75–82.
- 25 T. Kawahara, Y. Konishi, H. Tada, N. Tohge, J. Nishii and S. Ito, *Angew. Chem., Int. Ed.*, 2002, **41**, 2811–2813.
- 26 L. Li, P. A. Salvador and G. S. Rohrer, *Nanoscale*, 2014, **6**, 24–42.
- 27 L. Zhang, D. Jing, X. She, H. Liu, D. Yang, Y. Lu, J. Li, Z. Zheng and L. Guo, *J. Mater. Chem. A*, 2014, **2**, 2071–2078.
- 28 H. Zhu, Z. Zheng, X. Gao, Y. Huang, Z. Yan, J. Zou, H. Yin, Q. Zou, S. H. Kable, J. Zhao, Y. Xi, W. N. Martens and R. L. Frost, *J. Am. Chem. Soc.*, 2006, **128**, 2373–2384.
- 29 A. J. Paula, M. A. Zaghet, E. Longo and J. A. Varela, *Chem.–Eur. J.*, 2008, **2008**, 1300–1308.
- 30 A. Yu, J. Qian, L. Liu, H. Pan and X. Zhou, *Appl. Surf. Sci.*, 2012, **258**, 3490–3496.
- 31 J. H. Jung, C.-Y. Chen, W.-W. Wu, J.-I. Hong, B. K. Yun, Y. Zhou, N. Lee, W. Jo, L.-J. Chen, L.-J. Chou and Z. L. Wang, *J. Phys. Chem. C*, 2012, **116**, 22261–22265.
- 32 R. G. Pearson, *Coord. Chem. Rev.*, 1990, **100**, 403–425.
- 33 R. G. Pearson, *J. Am. Chem. Soc.*, 1963, **85**, 3533–3539.
- 34 A. G. Volkov, S. Paula and D. W. Deamer, *Bioelectrochem. Bioenerg.*, 1997, **42**, 153–160.
- 35 N. Li, L. Zhang, Y. Chen, M. Fang, J. Zhang and H. Wang, *Adv. Funct. Mater.*, 2012, **22**, 835–841.
- 36 R. Shannon, *Acta Crystallogr., Sect. A: Cryst. Phys., Diffr., Theor. Gen. Crystallogr.*, 1976, **32**, 751–767.
- 37 L. Pan, Y. Wang, X. Wang, H. Qu, J. Zhao, Y. Li and A. Gavriluk, *Phys. Chem. Chem. Phys.*, 2014, **16**, 20828–20833.
- 38 J. Yan, G. Wu, N. Guan and L. Li, *Appl. Catal., B*, 2014, **152–153**, 280–288.
- 39 K. Yoshimura, T. Miki, S. Iwama and S. Tanemura, *Thin Solid Films*, 1996, **281–282**, 235–238.
- 40 M. Kouhnavard, S. Ikeda, N. A. Ludin, N. B. Ahmad Khairudin, B. V. Ghaffari, M. A. Mat-Teridi, M. A. Ibrahim, S. Sepeai and K. Sopian, *Renewable Sustainable Energy Rev.*, 2014, **37**, 397–407.
- 41 N. Satoh, T. Nakashima, K. Kamikura and K. Yamamoto, *Nat. Nanotechnol.*, 2008, **3**, 106–111.
- 42 S. A. O'Neill, I. P. Parkin, R. J. H. Clark, A. Mills and N. Elliott, *J. Mater. Chem.*, 2003, **13**, 2952.
- 43 J.-M. Jehng and I. E. Wachs, *Catal. Today*, 1990, **8**, 37–55.
- 44 X. Chen, L. Liu, P. Y. Yu and S. S. Mao, *Science*, 2011, **331**, 746–750.
- 45 L. Zhang, T. Jiang, S. Li, Y. Lu, L. Wang, X. Zhang, D. Wang and T. Xie, *Dalton Trans.*, 2013, 12998–13003.
- 46 H. Zhu, X. Chen, Z. Zheng, X. Ke, E. Jaatinen, J. Zhao, C. Guo, T. Xie and D. Wang, *Chem. Commun.*, 2009, 7524–7526.
- 47 Z. Zheng, J. Zhao, H. Liu, J. Liu, A. Bo and H. Zhu, *ChemCatChem*, 2013, **5**, 2382–2388.
- 48 D. Jiang, W. Wang, E. Gao, L. Zhang and S. Sun, *J. Phys. Chem. C*, 2013, **117**, 24242–24249.
- 49 A. Yamamoto, Y. Mizuno, K. Teramura, T. Shishido and T. Tanaka, *Catal. Sci. Technol.*, 2013, **3**, 1771.
- 50 T. A. Westrich, K. A. Dahlberg, M. Kaviany and J. W. Schwank, *J. Phys. Chem. C*, 2011, **115**, 16537–16543.
- 51 M. Janus, E. Kusiak-Nejman and A. W. Morawski, *React. Kinet., Mech. Catal.*, 2012, **106**, 289–295.
- 52 F. Althoff, K. Benzing, P. Comba, C. McRoberts, D. R. Boyd, S. Greiner and F. Keppler, *Nat. Commun.*, 2014, **5**, 4205.
- 53 M. Zhang, Q. Wang, C. Chen, L. Zang, W. Ma and J. Zhao, *Angew. Chem., Int. Ed.*, 2009, **48**, 6081–6084.
- 54 Q. Wang, M. Zhang, C. Chen, W. Ma and J. Zhao, *Angew. Chem., Int. Ed.*, 2010, **49**, 7976–7979.
- 55 C. L. Hawkins, D. I. Pattison and M. J. Davies, *Amino Acids*, 2003, **25**, 259–274.
- 56 C. L. Hawkins and M. J. Davies, *Free Radical Biol. Med.*, 2005, **39**, 900–912.
- 57 V. Augugliaro, T. Caronna, V. Loddo, G. Marci, G. Palmisano, L. Palmisano and S. Yurdakal, *Chem.–Eur. J.*, 2008, **14**, 4640–4646.
- 58 S. Yurdakal, G. Palmisano, V. Loddo, V. Augugliaro and L. Palmisano, *J. Am. Chem. Soc.*, 2008, **130**, 1568–1569.
- 59 R. Kydd, W. Y. Teoh, J. Scott, D. Ferri and R. Amal, *ChemCatChem*, 2009, **1**, 286–294.
- 60 K. Takanabe and K. Domen, *ChemCatChem*, 2012, **4**, 1485–1497.